



A photo-excited electron transfer hyperchannel constructed in Pt-dispersed pyrimidine-modified carbon nitride for remarkably enhanced water-splitting photocatalytic activity



Xixiong Jin^{a,b}, Lingxia Zhang^{a,b,*}, Xiangqian Fan^{a,b}, Jianjian Tian^{a,b}, Min Wang^{a,b}, Jianlin Shi^{a,b,*}

^a State Key Laboratory of High Performance Ceramics and Superfine Microstructure, Shanghai Institute of Ceramics, Chinese Academy of Sciences, 1295 Dingxi Road, Shanghai 200050, People's Republic of China

^b University of Chinese Academy of Sciences, 19A Yuquan Road, Beijing 100049, People's Republic of China

ARTICLE INFO

Keywords:

Electron transfer
Carbon nitride
Copolymer
Photocatalytic water-splitting
Hydrogen evolution

ABSTRACT

Electron transfer kinetics plays a crucial role in water-splitting hydrogen evolution reaction, and accelerating the electron transfer while preventing charge recombination are one of the key factors in improving solar-fuel conversion. Here, we report the construction of a photo-excited electron transfer hyperchannel in Pt-dispersed pyrimidine-modified carbon nitride (PMCN) for remarkably enhanced water-splitting photocatalytic activity. The electrophilic pyrimidine groups were incorporated in polymeric carbon nitride (CN) to withdraw photo-excited electrons upon illumination and in the meantime donate the electrons to the wherein anchored Pt particles, providing fast electron transfer hyperchannels across the catalyst interface, which greatly promoted the photo-excited electron/hole separation and prevented their recombination. As a result, Pt-anchored PMCN exhibited remarkably enhanced photocatalytic performance, with the highest H₂ evolution under visible light irradiation reaching 3279.7 μmol h⁻¹ g⁻¹ and AQY% being 6% at 420 nm, 15.3 times higher than that of CN. The construction of electron transfer hyperchannel introduced a novel, facile and effective strategy to promote charge separation, presenting a new viewpoint for the rational design of photocatalysts to achieve improved solar-fuel conversion.

1. Introduction

Photocatalysis is considered as a promising strategy to effectively achieve renewable clean fuel from solar energy [1]. However, the currently low conversion efficiency keeps the technology years away from practical application [2–4]. The main photocatalytic processes of charge excitation, separation, transfer and subsequent participation in reduction/oxidation reactions have been widely studied [5]. It has been pointed out that the reduction half-reaction triggered by photo-excited electrons plays a decisive role in water-splitting hydrogen evolution reaction, and accelerating the electron transfer while suppressing their recombination with the holes are the critical issues for maximizing photocatalytic efficiency [6]. Accordingly, electron transfer kinetics should be fully studied and an effective strategy should be developed to accelerate electron transfer while preventing charge recombination at the same time.

Deployment of metal cocatalysts on the surface of photocatalysts is a general strategy to prevent charge recombination. As the most

commonly used cocatalyst in photocatalysis, platinum (Pt) is known for its extraordinary ability in accumulating photo-excited electrons and prolonging their lifetime. Typically, the electron transfer from Pt particles to protons is adequately efficient, however, the electron transfer from photocatalyst to metal particles is the rate-limiting step during the charge transfer, thus having a determining impact on the photocatalytic activity [7,8]. Hence, the metal-support interaction (MSI) becomes a much more important part to be considered in the synergistic photocatalytic mechanism [7,8]. Considering that the electron transfer from photocatalyst to noble metal particles such as Pt nanoparticles is currently still one of the most efficient way in minimizing fast recombination and energy dissipation of photo-excited electrons, it is of great importance to create a hyperchannel between the photocatalyst and the metal nanoparticles that is capable of readily trapping and then immediately transferring electrons to wherein-bound Pt particles for the surface water-reduction reaction.

Unfortunately, however, the effective metal cocatalyst nanoparticles' binding onto the semiconductor matrix is crucially important

* Corresponding author at: State Key Laboratory of High Performance Ceramics and Superfine Microstructure, Shanghai Institute of Ceramics, Chinese Academy of Sciences, 1295 Dingxi Road, Shanghai 200050, People's Republic of China.

E-mail addresses: zhlingxia@mail.sic.ac.cn (L. Zhang), jshi@mail.sic.ac.cn (J. Shi).

in constructing such a hyperchannel, which will largely suffer from their inefficient connection on the surface of semiconductors, leaving impassable gap for electron transfer and resultant less separated electrons as active sites for photocatalytic reaction. Hetero-semiconductor can help efficiently separate charges driven by potential difference or serve as buffer mediator facilitating electron transfer [9–12]. Unfortunately, the electron transfer in the composites only takes place at the interface between semiconductors, and the diffusion distance of electrons is mostly dependent on the interface thickness or the particle size of semiconductor-cocatalysts [12–14]. Recently, our group has developed a series of intramolecular conjugated copolymer photocatalysts based on polymeric graphitic carbon nitride (CN) [9,10,12–14], which translates the interface to intra-molecule heterostructure and is proven to be an effective approach to achieve efficient separation and mobility of charge carriers. Based on our well-established copolymerization methodology, we here chose 2,5-dibromopyrimidine monomer to synthesize an intramolecular conjugated copolymer photocatalyst, pyrimidine-modified carbon nitride (PMCN). Pyrimidine groups could greatly extend the electron delocalization and the structural distortion, activating the n to π^* transfer of electrons in CN [15,16]. Owing to the high electron affinity of aromatic C=C bonds, pyrimidine groups are largely prone to capture electrons from CN network upon illumination and maintain them at emission states, which will then immediately transfer to electron acceptors (e.g. Pt) and subsequently onward to protons for photocatalytic water reduction. Thus, an efficient and seamless hyperchannel from the CN matrix to the metal nanoparticle are constructed across the catalyst interface for accelerating electron transfer (Fig. 1). X-ray photoelectron spectroscopy (XPS) and transmission electron microscopy (TEM) reveal the strong MSI between Pt particles and pyrimidine groups. Electron transfer dynamic analysis based on time-resolved photoluminescence decay spectra (TR-PL) and transient absorption kinetics (TA) evidence the promoted electron transfer through the pyrimidine hyperchannel between PMCN and Pt. The hyperchannel in this Pt-anchored intramolecular conjugated polymer significantly accelerates the electron transfer, providing more active electrons on the Pt nanoparticles and consequently offering substantially enhanced efficiency in solar-fuel conversion.

2. Experimental section

2.1. Material preparation

The pyrimidine-modified carbon nitrides (PMCN) were prepared by heating 20 g urea and a certain amount of 2,5-dibromopyrimidine (50 mg, 100 mg, 150 mg) in an alumina crucible to 550 °C at the heating

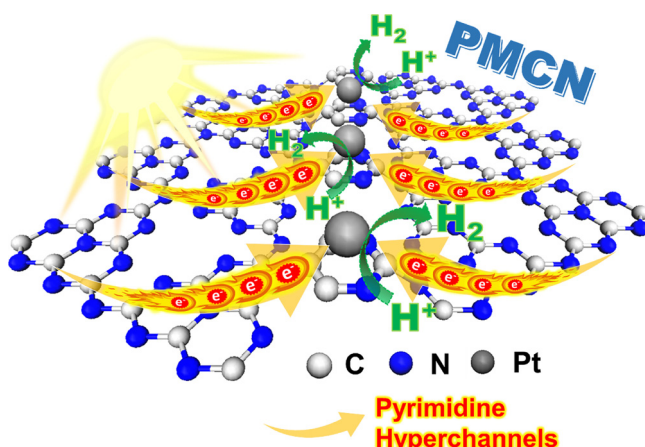


Fig. 1. Schematic illustration of pyrimidine-hyperchannel across the catalyst interface for accelerating electron transfer.

rate of 5 °C min⁻¹ and keeping at that temperature for 2 h prior to cooling. Then, the light-yellow products were collected and grinded into powder, denoted as PMCN-x, where x represents the amount of 2,5-dibromopyrimidine added. In comparison, pristine carbon nitride (denoted as CN) was synthesized by the same thermal treatment using 20 g urea as precursor only. All the as-prepared products were successively rinsed and washed using distilled water and ethanol 3 times, respectively, to remove residual precursors before further use.

2.2. Characterization

Fourier transform infrared spectra (FT-IR) were obtained using KBr pellets on a ThermoFischer Nicolet IS10 spectrometer. X-ray photo-electron spectroscopy (XPS) measurements were performed on a Thermo Scientific Escalab 250 spectrometer with Al K α radiation and the binding energies for the high resolution spectra were calibrated by setting C1s to 284.6 eV. ¹H MAS and ¹³C CP/MAS NMR experiments were performed on Bruker AVANCE III 600 spectrometer at a resonance frequency of 600.1 MHz and 150.9 MHz, respectively. ¹H MAS NMR spectra were recorded using a 4 mm MAS probe at a spinning rate of 14 kHz. A $\pi/2$ pulse length of 2.57 μ s and a recycle delay of 5 s were used for the ¹H MAS NMR experiments. ¹³C CP/MAS NMR spectra were recorded using a 4 mm MAS probe and a spinning rate of 14 kHz. A contact time of 2 ms, a recycle delay of 5 s were used for the ¹H-¹³C CP/MAS measurement. The chemical shifts of ¹H and ¹³C were externally referenced to TMS. The crystal structures of samples were investigated by X-ray diffraction (XRD; Rigaku D/Max 2200PC) with Cu K α radiation operated at 40 kV of acceleration voltage and 40 mA of applied current. The scanning rate was maintained at 4° min⁻¹ in the 2θ range of 10–80°. The morphology of the samples was recorded by transmission electron microscopy (TEM; FEI Tecnai G² F20) at an acceleration voltage of 200 kV. The Pt content was measured by Inductively Coupled Plasma Atomic Emission Spectroscopy (ICP-AES) on a Vista AX analyzer. The N₂ adsorption and desorption measurements were performed using Micromeritics Tristar 3000 at 77 K. The photoluminescence (PL) spectra of the samples were obtained by Edinburgh Instruments FLSP-920 fluorescence spectrophotometer with an excitation wavelength of 400 nm at room temperature. UV-vis absorption spectroscopy was examined on a Shimadzu UV-3600 spectrometer, using BaSO₄ as reference. Time-resolved PL decay spectra were measured on a HORIBA Scientific Fluoro-Cube. The instrument worked on the principle of time-correlated single-photon counting (TCSPC) (λ_{ex} = 360 nm). The femtosecond TA kinetic experiment was conducted on an automated data acquisition transient absorption spectrometer (Ultrafast, Helios). A femtosecond Ti/Sapphire regenerative amplifier laser system (CPA-2010, Clark-MXR) was used as amplifier seeded with the laser output from the oscillator and generated about 100 fs pulse at 800 nm with a repetition rate of 1 kHz. 70% of the amplified 800 nm output was used to barium boron oxide crystal second harmonic generator to obtain the laser of 400 nm as pump, and the probe pulse was obtained using the remaining 30% of the amplified 800 nm output which was focused on a sapphire crystal plate (with a thickness of 2.3 mm) to generate a white-light continuum spectrum in the range of 600–780 nm. The pump and probe beams were focused on the sample and kept the temporal and spatial overlap at the sample. The signal was recorded by detecting the intensity of the probe light.

2.3. Photocatalytic hydrogen evolution test

The H₂ evolution test under visible light was carried out in a Pyrex top-irradiation reaction vessel. A 300 W xenon lamp (CEL-HXF300, Ceaulight, Beijing) was used as light source. A 420 nm cut-off filter was chosen as a visible light source, and the light intensity was 225 mW cm⁻² (tested by FieldMax II TO, Coherent). 50 mg of photocatalyst was dispersed in 100 mL of deionized water, along with 10 mL of triethanolamine as sacrificial agent. Pt was loaded by in situ photo-deposition

adding 0.5 mL H_2PtCl_6 (3 mg mL^{-1}) as the precursor. The reactor was swept by nitrogen flow for 15 min to remove the dissolved oxygen prior to the irradiation experiment. The temperature of the reaction suspension was maintained at 10 °C by a flow of cooling water during the photocatalytic reaction. 1 mL evolved gases were extracted from the reactor every hour and injected into gas chromatography (Techcomp GC7900, equipped with TCD and 5 Å molecular sieve columns) to analyze. The AQY was calculated according to the following formula:

$$\begin{aligned}\text{nAQY (\%)} &= \frac{\text{number of reacted electrons}}{\text{number of incident photons}} \times 100 \\ &= \frac{\text{number of evolved H}_2 \text{ molecules} \times 2}{\text{number of incident photons}} \times 100\end{aligned}$$

2.4. Electrochemical characterizations

The electrochemical characterizations were performed on a CHI 760e electrochemical workstation (Chenhua Instrument, Inc.) in a standard three-electrode system consisting of Pt wire as counter electrode, Ag/AgCl (in saturated KCl) as reference electrode and sample-coated ITO as working electrode. Na_2SO_4 (0.2 M) aqueous solution was used as the electrolyte. The working electrode was prepared as follows: 20 mg of the grinded sample was mixed with 40 mg iodine, followed by adding acetone to full and sonicating the slurry for 30 min. Then, the dispersion was transferred into a 20 mL beaker and two pieces of 2 cm × 1.5 cm ITO glass were sunk into the dispersion with 10 V applied voltage for 10 min. Finally, the ITO glass with sample film was calcined at 150 °C for 7 h. EIS curves were obtained at -0.4 V vs Ag/AgCl. Irradiation used in the photocurrent tests was from a Xe lamp with a UV filter ($\lambda > 420 \text{ nm}$) with the bias at 0.2 V vs Ag/AgCl.

3. Results and discussion

3.1. The construction of a photo-excited electron transfer hyperchannel in Pt-dispersed pyrimidine-modified carbon nitride

The pyrimidine-modified carbon nitride (PMCN) was synthesized via a Schiff base reaction using urea and 2,5-dibromopyrimidine as precursors. After gradual polycondensation and structural rearrangement, the precursors were copolymerized to an intramolecular

copolymer as illustrated in Fig. 2a. The structure of the as-synthesized PMCN-x were verified by FT-IR spectra, ^1H MAS NMR spectra and XPS (Fig. 2b-d). The FT-IR absorption peak located at 1506 cm^{-1} corresponding to aromatic C=C bonds (Fig. 2b) as well as two intense ^1H MAS NMR signals at 1.54 and 4.03 ppm corresponding to the H atoms attached with graphitic carbon (Fig. 2c), evidence the existence of pyrimidine groups in PMCN-100. In N1s XPS spectra, the percentage of N-(C)_3 increases from 25.57% in CN to 35.24% in PMCN-100, which indicates that there are higher amount of tertiary nitrogen species in PMCN-100. This increasing amount of N-(C)_3 in PMCN is believed to originate from the nitrogen atoms in heptazine groups bonded to the terminal carbon atoms of pyrimidine groups as illustrated in Fig. 2d [17,18]. Note that the binding energy of N-(C)_3 and N-(H)_2 both positively shift, which arises from the structural distortion and chemical environment change brought by the incorporation of pyrimidine groups. In the meantime, the main tri-s-triazine structure is well-preserved in PMCN (Figure S1-S6). The above results confirm that pyrimidine groups have been successfully incorporated into CN network rather than adsorbed on the surface of CN, and they are mainly located at the edges and joints of tri-s-triazine units, forming an intramolecular heterostructure. The extensive chemical bonding between CN and pyrimidine groups ensures the smooth and rapid intramolecular electron transfer from CN matrix to pyrimidine groups, which also improves the visible-light response and prevents charge recombination to certain extents (Figure S7-10). These results confirm that the incorporation of pyrimidine groups has successfully modified the electronic structure of CN by greatly extending π -conjugation and withdrawing more electrons outward to valence band. As a result, the valence band position up-shifts and the band-gap is accordingly narrowed, leading to the enhanced visible light absorption and the improved photocatalytic performance.

The well-dispersed morphology of anchored Pt particles after *in-situ* photodeposition can be an intuitive indicator of the electron rich zone on the catalyst surface [19]. Therefore, Pt-dispersed CN and PMCN-100 (denoted as CN-Pt and PMCN-100-Pt) are further characterized. It is exhibited in Fig. 3a that Pt particles are deposited randomly on the surface of CN and mainly present as grown clusters of around 30–50 nm in size. However, Pt particles of smaller than 10 nm are much more evenly dispersed on the surface, and more preferentially deposited on the edges of PMCN-100 sheets (Fig. 3b). As above mentioned,

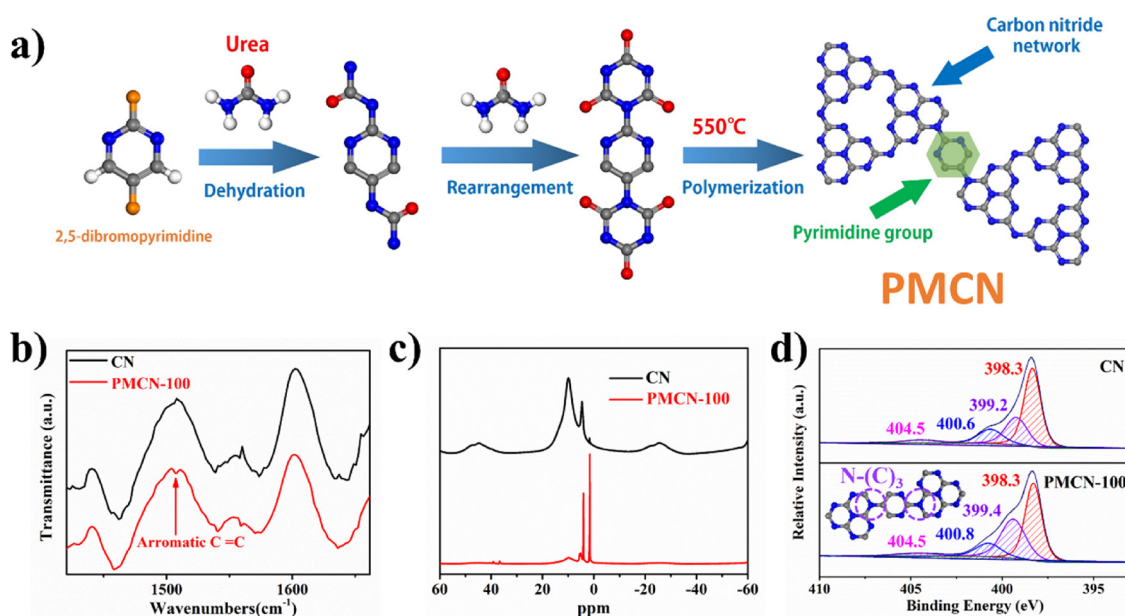


Fig. 2. a) Copolymerization schematics between 2,5-dibromopyrimidine and carbon nitride to form PMCN. b) High resolution FT-IR spectra of CN and PMCN-100. c) ^1H MAS NMR spectra of CN and PMCN-100. d) High-resolution N1s XPS spectra of CN and PMCN-100.

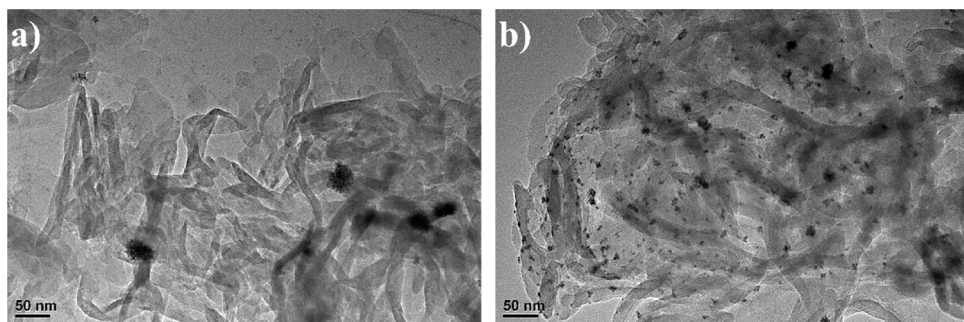


Fig. 3. TEM images of a) CN-Pt and b) PMCN-100-Pt.

pyrimidine groups are located on the edges and joints of PMCN copolymer, evidencing that the pyrimidine groups are indeed electron-rich sites with high reductive potential to reduce Pt^{4+} and in-situ anchor Pt nanoparticles. In other words, pyrimidine groups are more inclined to grab electrons from CN upon illumination, then immediately reduce PtCl_6^{2-} and seamlessly anchor Pt particles to the pyrimidine groups. This enhanced metal-support interaction between pyrimidine groups and Pt particles, as well as the substantial incorporation of pyrimidine groups into CN network, makes pyrimidine groups as junction points between Pt particles and CN matrix, facilitating the swift transfer of photo-excited electrons from CN matrix to Pt particles via pyrimidine hyperchannels.

In C1s XPS spectra of CN-Pt and PMCN-100-Pt (Fig. 4a), two original peaks at 287.9 eV and 284.6 eV are assigned to the aromatic C=N bonds and graphitic carbon atoms, respectively. A new peak can be found at 285.8 eV and assigned to the sp^2 carbon attached to Pt particles [20]. Pt4f XPS spectra were used to characterize the different chemical states of the *in-situ* deposited Pt on CN and PMCN-100, which could be deconvoluted into two peaks located at ~70 eV and ~71 eV, representing Pt° and Pt^{2+} , respectively (Fig. 4c). According to the previous research, Pt° and Pt^{2+} species on the surface of CN are assigned to the metallic Pt with a PtO shell around it [21]. Pt° signals of CN-Pt (70.2 eV) and PMCN-100-Pt (70.1 eV) are similar with each

other, but a slight negative shift is present in PMCN-100-Pt. However, Pt^{2+} signal of PMCN-100-Pt exhibits a lower binding energy by 0.9 eV in comparison with that of CN-Pt. Additionally, O1s signal of PMCN-100-Pt shifts to higher binding energy comparing with that of PMCN-100, and yet a negative shift can be observed on CN-Pt (Fig. 4d). These results confirm that the Pt species has been photo-reduced to metallic states more thoroughly on the surface of PMCN-100 by inducing more photo-excited electrons onto PtCl_6^{2-} , agreeing well with TEM result. Moreover, in the N1s spectrum of PMCN-100 (Fig. 4b), the signal of sp^3 bridging nitrogen ($\text{N}-(\text{C})_3$) at 399.4 eV negatively shifts to 399.1 eV after Pt loading, suggesting the occurrence of electron transfer from bridging nitrogen atoms of carbon nitride matrix via pyrimidine groups to Pt particles on the surface. This indicates the incorporation of pyrimidine groups makes electrons transfer to Pt particles more effectively via pyrimidine hyperchannels than directly from CN matrix. Sum up all above discussions, pyrimidine groups are successfully incorporated into CN matrix via copolymerization strategy and indeed construct hyperchannels, enhancing metal-support interaction and effectively facilitating electron-donation from copolymer support via pyrimidine hyperchannel to Pt particles.

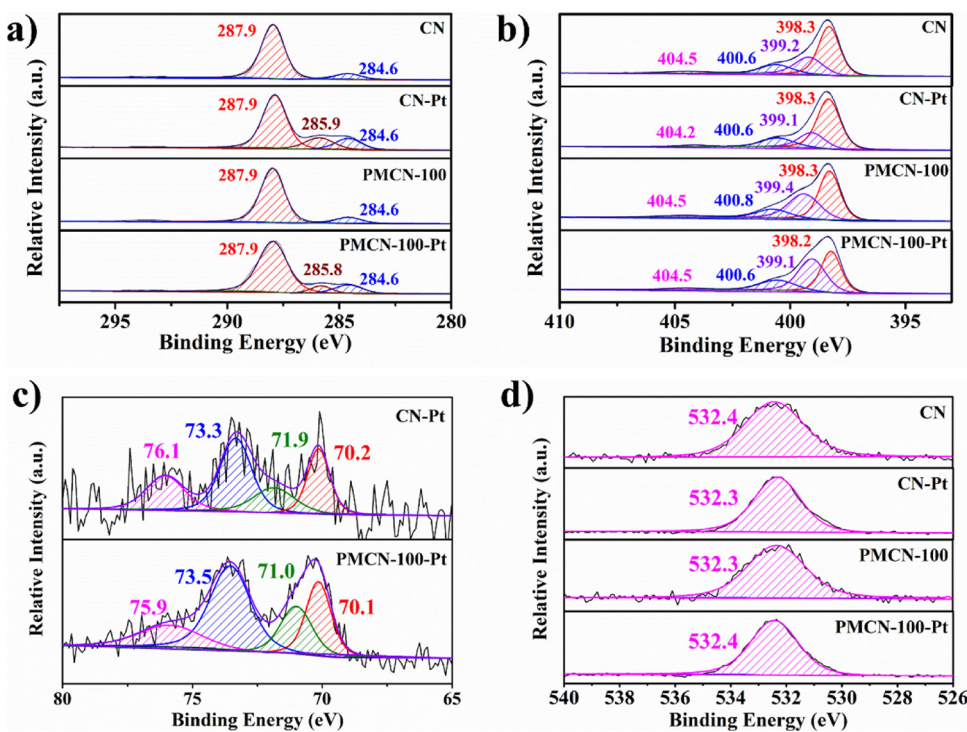


Fig. 4. High-resolution a) C1s, b) N1s and d) O1s XPS spectra of CN, CN-Pt, PMCN-100 and PMCN-100-Pt; c) Pt4f XPS spectra of CN-Pt and PMCN-100-Pt.

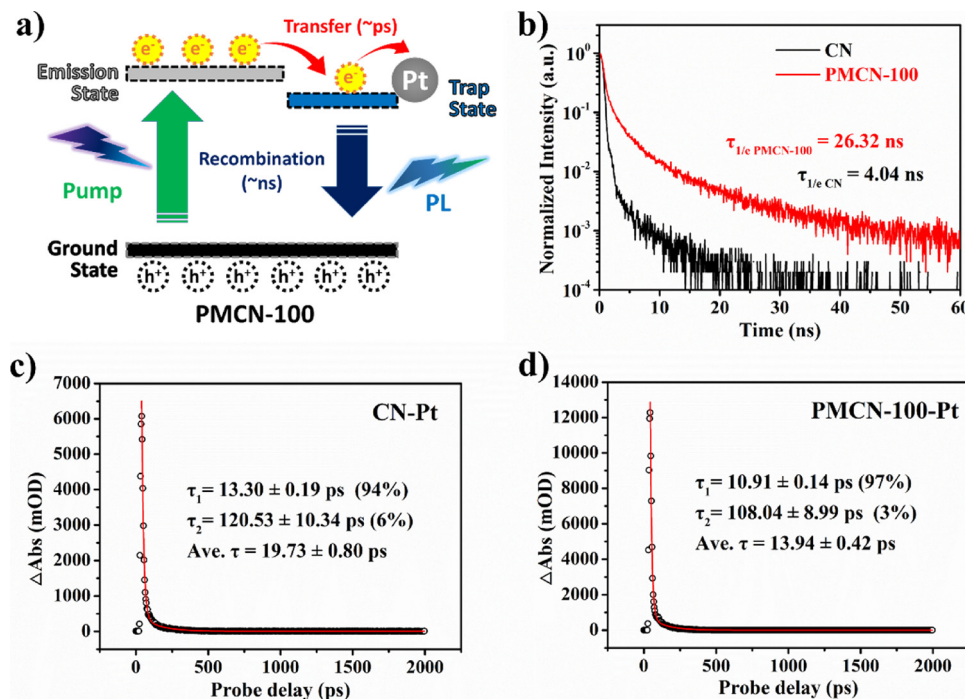


Fig. 5. a) Schematic illustration of the proposed mechanism for charge transfer in PMCN-100-Pt; b) Time-resolved PL decay spectra of CN and PMCN-100; Ultrafast TA kinetics of c) CN-Pt and d) PMCN-100-Pt probed at 420–800 nm (pumped at 400 nm).

3.2. Dynamic analysis of photo-excited electrons in pyrimidine hyperchannels

A proposed dynamic model of charge transfer in PMCN-100-Pt is illustrated in Fig. 5a. Once the photocatalyst is irradiated, electrons will be excited to the emission state and leave holes at the ground states. Without acceptor, the excited electrons will directly recombine with holes at the ground state to release luminescence or transfer to the nearby trap state then fall back into the ground state. The recombination usually occurs in nanosecond (ns), and yet the charge transfer takes place in a much more rapid timescale (picoseconds, ps) [22,23]. Thus, to further confirm how the construction of pyrimidine hyperchannels affects the electron transfer in Pt-dispersed PMCN, the recombination processes in the samples were recorded by time-resolved PL decay spectra (TR-PL) and the corresponding charge transfer processes were analyzed by transient absorption kinetics (TA) (Fig. 5b-d).

As illustrated in Fig. 5b, the TR-PL decay spectra show a 6.5-fold longer PL decay of PMCN-100 ($\tau_{1/e} = 26.32 \text{ ns}$) than that of CN ($\tau_{1/e} = 4.04 \text{ ns}$), indicating a longer charge lifetime and a slower charge recombination process in PMCN-100. The prolonged charge lifetime suggests that most photo-excited electrons at emission states are trapped in sufficient trap states formed on the surface of PMCN-100, followed by further transferring to Pt particles instead of instantly recombining with holes. This should be attributed to the excellent electron withdrawing capability of pyrimidine groups from CN, leading to the large delocalization of electronic states. However in pure CN, the trap states are mainly from the intrinsic structure defects, which are disorderly distributed and serve as active sites and also recombination sites at the same time, greatly diminishing the amount of active electrons and accelerating charge recombination. These results confirms that pyrimidine groups indeed possesses excellent ability to withdraw photo-excited electrons and maintain their emission states till further transfer to Pt particles and subsequently onward to protons.

Though photo-excited electrons are well-preserved in trap states, the deeply trapped electrons are inactive and not able to participate in photocatalytic process [23], making the charge transfer from trap states to Pt the limiting step of the hydrogen evolution reaction. Thus, the

charge transfer process from polymer matrix to Pt nanoparticles was further investigated on the basis of TA kinetics (Fig. 5c and d). Both CN-Pt and PMCN-100-Pt exhibit a rapid absorption peak at the early timescale after photoexcitation at 400 nm, suggesting the instantaneous direct excitation of electrons from ground states to emission states. The following TA signal decay is ascribed to the stimulated emission and photo-bleaching of the ground state absorption [23]. The decay curves can be fitted by exponential decays and described by two time constants: $\tau_1 = 13.30 \pm 0.19 \text{ ps}$ (94%) and $\tau_2 = 120.53 \pm 10.34 \text{ ps}$ (96%) for CN-Pt, while $\tau_1 = 10.91 \pm 0.14 \text{ ps}$ (94%) and $\tau_2 = 108.04 \pm 8.99 \text{ ps}$ (96%) for PMCN-100-Pt. The weighted average decay lifetime is $19.73 \pm 0.80 \text{ ps}$ for CN-Pt and $13.94 \pm 0.42 \text{ ps}$ for PMCN-100-Pt. The average decay lifetime can be an important but initial indicator for evaluating the charge transfer efficiency from the conduction band of semiconductor to the decorated metal nanoparticles [24,25]. It is observed that the average decay lifetime of PMCN-100-Pt is substantially shorter than that of CN-Pt, confirming that the electrons on the trap states of PMCN-100 can immediately transfer to Pt, more efficient than those in CN can do. The hyperchannel across the pyrimidine groups of PMCN to Pt nanoparticles significantly facilitate the electron transfer. The finding on the electron transfer pathway firmly supports the hyperchannel mechanism we here proposed in PMCN copolymer, which, as we believe, will be responsible for the remarkably enhanced photocatalytic activity of CN as presented in the following section.

3.3. Remarkably enhanced water-splitting photocatalytic activity of Pt-dispersed pyrimidine-modified carbon nitride

The photocatalytic performance was examined by evaluating the water-splitting hydrogen evolution rate of PMCN-x using triethanolamine (TEOA) as sacrificial agent to consume photo-excited holes ($V_{\text{water}}:V_{\text{TEOA}} = 10:1$). A dramatically enhanced hydrogen evolution rate up to $3279.7 \mu\text{mol h}^{-1} \text{ g}^{-1}$ is achieved on PMCN-100 after loading Pt particles under visible light irradiation, 15.3 times that on CN ($213.9 \mu\text{mol h}^{-1} \text{ g}^{-1}$) (Fig. 6a). The same increment was also demonstrated in the photocurrent responses (Figure S11). We presume that the

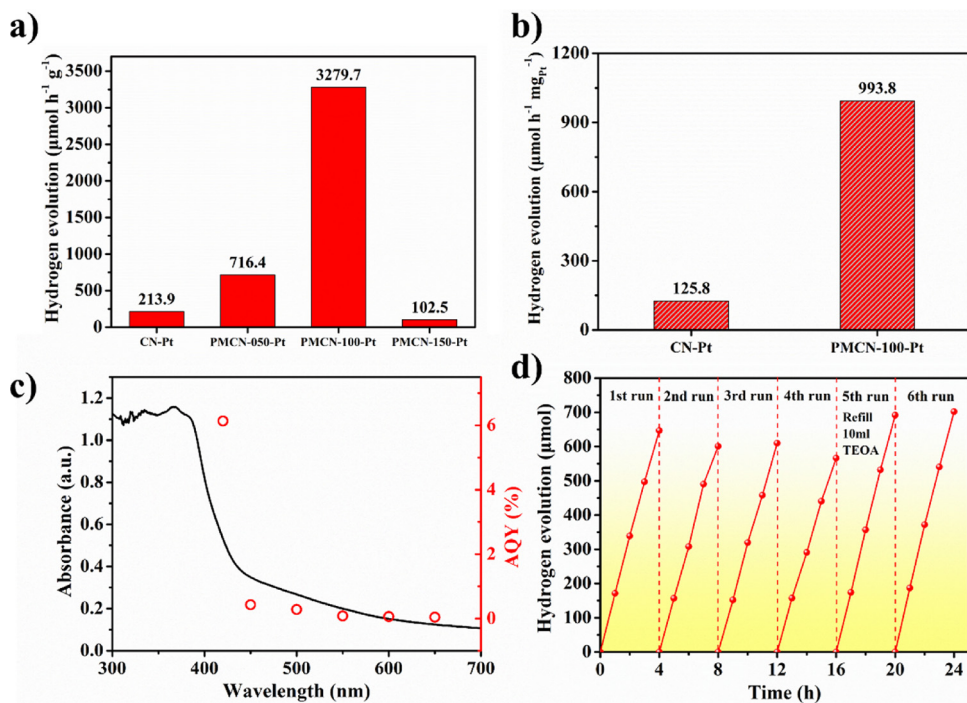


Fig. 6. a) Hydrogen evolution rate of CN-Pt and PMCN-x-Pt under visible light. b) Hydrogen evolution rates per mg Pt loaded on CN and PMCN-100. c) Wavelength-dependent apparent quantum yield of PMCN-100-Pt. d) Cycling stability evaluation of PMCN-100-Pt under visible light.

small amount of 2,5-dibromopyrimidine creates less hyperchannels, and the leading trap states in the system is still ascribed to the less effective intrinsic surface defects of CN. On the other hand, excessive 2,5-dibromopyrimidine addition in the precursors would result in the over-distortion of CN network and collapse of pore structure, creating discrete debris and compromising light-responsive activity of PMCN. Additionally, the corresponding hydrogen evolution rate per mg Pt particles loaded on PMCN-100 ($993.8 \mu\text{mol h}^{-1} \text{mg}_{\text{Pt}}^{-1}$) is also enhanced by 7.9 times that on CN ($125.8 \mu\text{mol h}^{-1} \text{mg}_{\text{Pt}}^{-1}$), exhibiting the higher utilization rate of Pt particles brought by the construction of pyrimidine hyperchannel (Fig. 6b). The apparent quantum yield (AQY) of PMCN-100-Pt reaches 6% at 420 nm, which fits well with its optical absorption spectrum and further confirms that the photocatalytic reaction is mainly driven by the photon energy of visible light (Fig. 6c). To further evaluate the stability of PMCN-100-Pt, a 24-hour cycling photocatalytic experiment was conducted under the same condition (Fig. 6d). In the first 16 h, a slight decrease of H_2 evolution rate from $167 \mu\text{mol h}^{-1}$ to $148 \mu\text{mol h}^{-1}$ was observed, which was most likely due to the quick consumption of TEOA. After refilling 10 mL TEOA at the 5th run, the H_2 evolution rate was back to $182 \mu\text{mol h}^{-1}$ and finally stabilized at $176 \mu\text{mol h}^{-1}$ at the 6th run, demonstrating the robust stability of PMCN-100. Moreover, the XRD pattern and FT-IR spectrum of PMCN-100-Pt change little after Pt loading, indicating that PMCN-100 is structurally and chemically stable during the photocatalytic reaction (Figure S12, 13). Combining all the data above, we can safely ascribe this dramatic enhancement in photocatalytic performance after Pt loading to the effect of pyrimidine hyperchannel in photo-excited electron transfers, resulting in the rapid electron transfer from PMCN to Pt particles, and subsequently boosting the photocatalytic activity and proton reduction, i.e., water-splitting.

4. Conclusion

In conclusion, we have developed an efficient copolymerization strategy for synthesizing pyrimidine-modified carbon nitride (PMCN), which provides a hyperchannel for photo-excited electron transfer from carbon nitride (CN) matrix to the anchored Pt nanoparticles. Owing to

the extraordinary electro-withdrawing ability of pyrimidine groups and its strong interaction with the Pt particles, such a hyperchannel has been evidenced to be capable of largely promoting the electron transfer across the catalyst interface, i.e., from the copolymer matrix to cocatalyst Pt, which is the limiting step during the photocatalytic reaction. Consequently, the Pt-loaded PMCN demonstrates a remarkably enhanced photocatalytic activity of an extra high hydrogen evolution rate of $3279.9 \mu\text{mol h}^{-1} \text{g}^{-1}$ and AQY of 6% at 420 nm, 15.3 times that of CN. This work not only provides an effective copolymerization strategy to modulate electronic configuration of CN, but also highlights the importance of metal-support interaction in the photocatalyst system, revealing the effectiveness of electron transfer hyperchannel construction in the rational design of photocatalysts for substantially elevated solar-fuel conversion.

Acknowledgment

We acknowledge financial supports from the National Key Basic Research Program of China (2013CB933200), National Natural Science Foundation of China (21177137).

Appendix A. Supplementary data

Supplementary material related to this article can be found, in the online version, at doi:<https://doi.org/10.1016/j.apcatb.2018.06.035>.

References

- [1] K. Fujishima, Honda, Electrochemical photolysis of water at a semiconductor electrode, *Nature* 238 (1972) 37–38.
- [2] F.E. Osterloh, Inorganic materials as catalysts for photochemical splitting of water, *Chem. Mater.* 20 (2008) 35–54.
- [3] Y. Qu, X. Duan, Progress, challenge and perspective of heterogeneous photocatalysts, *Chem. Soc. Rev.* 42 (2013) 2568–2580.
- [4] A. Kubacka, M. Fernández-García, G. Colón, Advanced nanoarchitectures for solar photocatalytic applications, *Chem. Rev.* 112 (2012) 1555–1614.
- [5] J. Low, J. Yu, M. Jaroniec, S. Wageh, A.A. Al-Ghamdi, Heterojunction photocatalysts, *Adv. Mater.* 29 (2017) 1601694.
- [6] W. Bi, X. Li, L. Zhang, T. Jin, L. Zhang, Q. Zhang, Y. Luo, C. Wu, Y. Xie, Molecular co-catalyst accelerating hole transfer for enhanced photocatalytic H_2 evolution, *Nat.*

Commun. 6 (2015) 8647.

[7] J. Shi, On the synergistic catalytic effect in heterogeneous nanocomposite catalysts, *Chem. Rev.* 113 (2013) 2139–2181.

[8] P.V. Kamat, Manipulation of charge transfer across semiconductor interface. A criterion that cannot be ignored in photocatalyst design, *J. Phys. Chem. Lett.* 3 (2012) 663–672.

[9] J. Tian, L. Zhang, X. Fan, Y. Zhou, M. Wang, R. Cheng, M. Li, X. Kan, X. Jin, Z. Liu, Y. Gao, J. Shi, A post-grafting strategy to modify g-C₃N₄ with aromatic heterocycles for enhanced photocatalytic activity, *J. Mater. Chem. A* 4 (2016) 13814–13821.

[10] X. Fan, L. Zhang, R. Cheng, M. Wang, M. Li, Y. Zhou, J. Shi, Construction of graphitic C₃N₄-based intramolecular donor-acceptor conjugated polymers for photocatalytic hydrogen evolution, *ACS Catal.* 5 (2015) 5008–5015.

[11] W. Che, W. Cheng, T. Yao, F. Tang, W. Liu, H. Su, Y. Huang, Q. Liu, J. Liu, F. Hu, Z. Pan, Z. Sun, S. Wei, Fast photoelectron transfer in (cring)-C₃N₄ plane heterostructural nanosheets for overall Water splitting, *J. Am. Chem. Soc.* 139 (2017) 3021–3026.

[12] R. Cheng, X. Jin, X. Fan, M. Wang, J. Tian, L. Zhang, J. Shi, Incorporation of N-doped reduced graphene oxide into pyridine-copolymerized g-C₃N₄ for greatly enhanced H₂ photocatalytic evolution, *Wuli Huaxue Xuebao/ Acta Phys. - Chim. Sin.* 33 (2017) 1436.

[13] X. Fan, L. Zhang, M. Wang, W. Huang, Y. Zhou, M. Li, R. Cheng, J. Shi, Constructing carbon-nitride-based copolymers via Schiff base chemistry for visible-light photocatalytic hydrogen evolution, *Appl. Catal. B Environ.* 182 (2016) 68–73.

[14] M. Li, L. Zhang, X. Fan, M. Wu, Y. Du, M. Wang, Q. Kong, L. Zhang, J. Shi, Dual synergistic effects in MoS₂/pyridine-modified g-C₃N₄ composite for highly active and stable photocatalytic hydrogen evolution under visible light, *Appl. Catal. B Environ.* 190 (2016) 36–43.

[15] W. Ho, Z. Zhang, W. Lin, S. Huang, X. Zhang, X. Wang, Y. Huang, Copolymerization with 2,4,6-triaminopyrimidine for the rolling-up the layer structure, tunable electronic properties, and photocatalysis of g-C₃N₄, *ACS Appl. Mater. Interfaces* 7 (2015) 5497–5505.

[16] Y. Chen, B. Wang, S. Lin, Y. Zhang, X. Wang, Activation of n- * transitions in two-dimensional conjugated polymers for visible light photocatalysis, *J. Phys. Chem. C.* 118 (2014) 29981–29989.

[17] J. Liu, Y. Liu, N. Liu, Y. Han, X. Zhang, H. Huang, Y. Lifshitz, S.T. Lee, J. Zhong, Z. Kang, Metal-free efficient photocatalyst for stable visible water splitting via a two-electron pathway, *Science* 347 (2015) 970–974.

[18] J. Lahaye, G. Nansé, A. Bagreev, V. Strelko, Porous structure and surface chemistry of nitrogen containing carbons from polymers, *Carbon N. Y.* 37 (1999) 585–590.

[19] V.W. hei Lau, V.W. zhi Yu, F. Ehrat, T. Botari, I. Moudrakovski, T. Simon, V. Duppel, E. Medina, J.K. Stolarczyk, J. Feldmann, V. Blum, B.V. Lotsch, Urea-modified carbon nitrides: enhancing photocatalytic hydrogen evolution by rational defect engineering, *Adv. Energy Mater.* 7 (2017) 1602251.

[20] S. Lalitha, P.T. Manoharan, X-ray photoelectron spectroscopic studies on some di-thiolate complexes, *J. Electron. Spectros. Relat. Phenom.* 49 (1989) 61.

[21] F. Fina, H. Ménard, J.T.S. Irvine, The effect of Pt NPs crystallinity and distribution on the photocatalytic activity of Pt-g-C₃N₄, *Phys. Chem. Chem. Phys.* 17 (2015) 13929–13936.

[22] H. Kasap, C.A. Caputo, B.C.M. Martindale, R. Godin, V.W.H. Lau, B.V. Lotsch, J.R. Durrant, E. Reisner, Solar-driven reduction of aqueous protons coupled to selective alcohol oxidation with a carbon nitride-molecular Ni catalyst system, *J. Am. Chem. Soc.* 138 (2016) 9183–9192.

[23] R. Godin, Y. Wang, M.A. Zwijnenburg, J. Tang, J.R. Durrant, Time-resolved spectroscopic investigation of charge trapping in carbon nitrides photocatalysts for hydrogen generation, *J. Am. Chem. Soc.* 139 (2017) 5216–5224.

[24] P. Yu, X. Wen, Y.C. Lee, W.C. Lee, C.C. Kang, J. Tang, Photoinduced ultrafast charge separation in plexcitonic CdSe/Au and CdSe/Pt nanorods, *J. Phys. Chem. Lett.* 4 (2013) 3596–3601.

[25] S. Kim, S. Lee, S. Kim, S. Kwon, K. Yee, H. Song, G. Somorjai, J. Park, Hot carrier-driven catalytic reactions on Pt–CdSe–Pt nanodumbbells and Pt/GaN under light irradiation, *Nano Lett.* 3 (2013) 1352–1358.